



Digital Image Colorimetric Detection of H₂O₂ Utilizing PEG/Ag/AgO Nanoparticles Derived from Tangerine Leaf Extract

Emre Yılmazoğlu^{1*} 

¹Istanbul University-Cerrahpaşa, Faculty of Engineering, Department of Chemical Engineering, 34320, Avcılar, Istanbul, Türkiye.

Abstract: Recent developments in biosensors based on digital platforms have primarily focused on enhancing rapid detection, flexibility, and selectivity through the utilization of nanomaterials. Despite these advances, the complexity of image colorimetric measurements continues to be a subject of interest. This study focused on the development of a new digital image colorimetric biosensor for real-time quantification of hydrogen peroxide (H₂O₂). The designed nanostructure-based sensor showed excellent selectivity and sensitivity, utilizing polyethylene glycol/Silver/Silver(II) oxide nanoparticles obtained from tangerine leaf extract (TLE/PEG/Ag/AgO NPs). The sensor's performance was validated using Ag/AgO NPs derived from tangerine leaf extract (TLE), demonstrating remarkable selectivity and sensitivity using a Red-Green-Blue (RGB)--based approach. Based on digital image colorimetric measurements of TLE/PEG/Ag/AgO NPs, a system for determining H₂O₂ was established in a linear range of 2.0–100.0 µmol/L with a low limit of detection (LOD) of 1.82 µmol/L. This study not only presented a facile strategy for the design of the digital image colorimetric TLE/PEG/Ag/AgO NPs-based biosensor but also shed light on the remarkable potential of smartphone sensing devices based on nanosensor technology. These sensors offer fresh perspectives and multidisciplinary approaches to visually sensitive sensing in a range of applications, such as biomedical diagnostics, security screening, and environmental monitoring.

Keywords: Digital biosensor, Image colorimetric sensor, Silver nanoparticles, Green sensor.

Submitted: February 19, 2024. **Accepted:** July 1, 2024.

Cite this: Yılmazoğlu E. Digital Image Colorimetric Detection of H₂O₂ Utilizing PEG/Ag/AgO Nanoparticles Derived from Tangerine Leaf Extract. JOTCSA. 2024;11(3): 1303-12.

DOI: <https://doi.org/10.18596/jotcsa.1439951>

***Corresponding author's E-mail:** emre.yilmazoglu@iuc.edu.tr

1. INTRODUCTION

Nanotechnology involves the creation and utilization of materials that are one, two, or three-dimensional and range in scale from 1 to 100 nm, with high performance in physical, chemical, biological, optical, electrical, etc., for various purposes, especially in fields such as medicine, electronics, and the environment (1). These nanoscale materials have the advantage of being easily incorporated into the structure or metabolism of bulk materials due to their small volume. In addition, their high energy and surface area make it easier and less expensive for them to exhibit desired qualities than it would be to change the bulk material's attributes (2,3).

Both organic and inorganic structures, such as metals or metal oxides, as well as polymers, lipids, and carbohydrates, can be used in the design of advanced NPs (4-6). High selectivity and stability are well-known characteristics of metal or metal oxide-

based NP sensors. Depending on their composition and form, these nanoparticles may also possess magnetic, fluorescent, anticancer, antibacterial, antifungal, antiviral, anti-inflammatory, and wound-healing properties (7,8). These properties render them extremely valuable in a multitude of applications, such as medical imaging, biomedical device coatings, wound dressings, and drug delivery systems.

The development of biosensors based on inorganic nanoparticles (NPs) has garnered significant attention in recent years in biomedical applications. These sensors, surpassing traditional counterparts, offer distinct advantages, especially in the early diagnosis of diseases. Key benefits encompass fast response times, portability, sensitivity, selectivity, reusability, and affordability (9-11). Nanostructure-based biosensors exhibit effectiveness in detecting a broad spectrum of biomolecules, ranging from antibodies, proteins, and carbohydrates to enzymes,

hormones, nucleic acids, and microorganisms. The integration of nanoparticles into biosensor design plays a crucial role in enhancing the sensitivity and selectivity of measurements, significantly elevating biosensor performance. It is known that Ag NPs possess a broad application potential, particularly in the realms of medicine and electronics, owing to their conductivity, antimicrobial properties, and biocompatibility (12-14). Numerous research have studied the usage of Ag NPs in biological contexts, examining their various forms and sizes. Specifically, a multitude of studies have reported on the sensitive detection of biomarkers associated with the early diagnosis of cancer using Ag NPs. H_2O_2 is among the most prevalent reactive oxygen species in medical metabolism research. Imbalances in reactive species induce oxidative stress in the body, potentially resulting in various illnesses, including those related to the immune system, such as cancer. Thus, a prompt and cost-effective measurement of chemical concentrations, such as H_2O_2 , in biological settings provides a distinct advantage for diagnosing illnesses.

With the advent of green chemistry, the utilization of biological sources for nanoparticle synthesis has grown in popularity. Microorganisms and plant extracts are used to create abundant, affordable, biodegradable, and biocompatible compounds through green synthesis. This green synthesis, which uses a bottom-up methodology, involves using the functional groups found in biological components to produce nanoparticles from metal ions. Especially biological wastes containing compounds with capping/reducing effects can be used for this purpose, increasing the added value. Moringa (*Moringa oleifera*), ginger (*Zingiber officinale*), thyme (*Thymus vulgaris*), oregano (*Origanum vulgare*), rice (*Oryza sativa*), Mexican poppy (*Argemone mexicana*), *Alpinia katsumadai*, blue pea (*Clitoria ternatea*), black nightshade (*Solanum*

nigrum), China hibiscus (*Hibiscus rosa-sinensis*), Aniseed (*Pimpinella anisum*), ivy gourd (*Coccinia grandis*), Indian gooseberry (*Phyllanthus emblica*), satsuma mandarin (*Citrus unshiu*), mandarin (*Citrus reticulata*), sweet orange (*Citrus sinensis*), lemon (*Citrus limon*) and many other plants can be used in the green synthesis of Ag nanoparticles (15-31).

In this study, green Ag/AgO NPs were synthesized using a simple sonochemical method, incorporating biowaste tangerine leaf extract (TLE) and biodegradable polyethylene glycol (PEG). The biodegradable TLE/PEG/Ag/AgO NPs were characterized using transmission electron microscopy (TEM), Fourier-transform infrared spectroscopy (FTIR), and X-ray diffraction (XRD) methods. The performance of the proposed H_2O_2 -sensitive biosensor was assessed through the RGB method, employing a mobile phone with a digital color approach. This approach aimed to develop a sensor that is both sensitive to H_2O_2 and environmentally friendly.

2. EXPERIMENTAL SECTION

2.1. Materials

Mandarin (*Citrus reticulata*), sourced from Mersin, Turkey, was obtained from a local market in Istanbul. Various materials, including ethyl alcohol, PEG400, epichlorohydrin, $AgNO_3$, acetone, hexane, toluene, glucose, isopropyl alcohol (IPA), and H_2O_2 , were purchased from Merck Company (Germany).

2.2. Preparation of TLE/PEG/Ag/AgO NPs

The mandarin leaves underwent a thorough cleansing with distilled water and was subsequently dried in an oven at 80 °C for an hour. Following this, 40 g of dry plant material was treated with a 100 ml solution consisting of 80% (v/v) ethyl alcohol and water, employing an ultrasonic bath at 50 °C for 2 hours. The extracts were filtered with filter paper.

Table 1: Variations in composition for the preparation of green TLE/PEG/Ag/AgO NPs.

Code	Extract	PEG400	Epichlorohydrin	$AgNO_3/NaOH$
TLE/PEG	20 mL	-	-	-
TLE/PEG	20 mL	0.1 g	0.02 g	-
TLE/PEG/Ag/AgO NPs	20 mL	0.1 g	0.02 g	0.012 M/0.1 M

Different samples with distinct compositions were prepared (Table 1). Initially, TLE extracts were procured, followed by the addition of 0.1 g PEG400 to 20 mL of the extract in a sequential step. Subsequently, 0.02 g of epichlorohydrin was introduced and stirred at 700 rpm using a magnetic stirrer. Finally, to obtain TLE/PEG/Ag/AgO NPs, 10 mL of 0.012 M $AgNO_3$ and 2 mL of 0.1 M NaOH solution were added, and the sample was sonicated for 30 minutes. Remarkably, a discernible color change was observed in all solutions within the latest 5 minutes of the process.

2.3. Characterization

The morphology and chemical properties of the synthesized TLE/PEG/Ag/AgO NPs were evaluated through various characterization techniques. High-resolution transmission electron microscopy

(HRTEM) with an acceleration voltage of 100 kV, utilizing the HighTech HT7700 instrument, was employed for morphological analysis. X-ray diffraction analysis (XRD) was conducted using Malvern Panalytical Aeris 600W, with Cu K α radiation at 40 kV and 15 mA, providing insights into the crystallographic structure. Fourier transform infrared spectroscopy (FTIR) was performed in the frequency range of 400 to 4000 cm^{-1} to assess the functional groups present in the synthesized TLE/PEG/Ag/AgO NPs.

The TEM images were processed and analyzed using ImageJ software to determine the particle dispersion of TLE/PEG/Ag/AgO NPs. For assessing the RGB color channels of smartphone cameras, we employed a Casper VIA F20 (Türkiye) smartphone equipped with cameras featuring resolutions of 48MP-5MP-2MP-

2MP. Additionally, the XRD data were utilized to calculate the crystallite size of the TLE/PEG/Ag/AgO NPs using the Debye-Scherer equation (2.1) (32).

$$\tau = K\lambda / \beta \cos\theta \quad (2.1)$$

where β is the full width at half-maximum (FWHM), K is the form factor equal to 0.9, and θ is the experimental Bragg angle of the diffraction peak of TLE/PEG/Ag/AgO NPs.

2.4. Calculations

In digital colorimetric analyses, diverse compounds such as acetone, hexane, toluene, glucose, IPA, and H_2O_2 were examined in concentrations ranging from 2.0 to 100.0 $\mu\text{mol/L}$. In a transportable box (20 cm*20 cm*5 cm), the sample and the smartphone camera were separated by 10 cm. Using the automated option without close-up or filter, the specimen was centered in the image. A high-quality image with a comparable light effect appeared after around ten seconds. Using the RGB color assessment, all digital-colorimetric observations of 2 mL of the green TLE/PEG/Ag/AgO NPs-digital biosensor were performed for 1 minute at 25 °C against 10 μM of the target analyte. Utilizing a camera-integrated colorimetric TLE/PEG/Ag/AgO NPs-biosensor on an F20 model smartphone, all photos were used to study the selective detection of H_2O_2 at a resolution of 1600 \times 1200 pixels, with data falling between for black color value [0,0,0] and for white color value [255,255,255]. An ImageJ color software was used to examine every image of the biosensors that had been developed. Using Eqs. 2.2–2.6 (33), the prepared TLE/PEG/Ag/AgO NPs-based biosensor's Euclidean distance (ΔE), response (S), limit of detection (LOD), and limit of quantification (LOQ) values were determined for the selective digital colorimetric detection of H_2O_2 .

$$\Delta E = \sqrt{(R_i - R_0)^2 + (G_i - G_0)^2 + (B_i - B_0)^2} \quad (2.2)$$

$$S = 100 \frac{X_c - X_0}{X_0 - X_{ref}} [\%] \quad (2.3)$$

$$S(\%) = m \log(C) + n \quad (2.4)$$

$$LOD = 3.3\sigma/m \quad (2.5)$$

$$LOQ = 10\sigma/m \quad (2.6)$$

Sample color values for red, green, and blue colors are represented as R_i , G_i , and B_i , respectively. R_0 , G_0 , and B_0 are the reference values for the colors. X_c is the concentration-related raw sensor signal, X_0 is the signal measured at zero concentration, and the X_{ref} is the reference signal value for each color channel (is equal to 255 for red and green, to 0 for blue). n is the intercept and m is the slope of the line equation between response (S) and base-10 logarithm of the concentration of the analyte (C). σ is the standard deviation value of the response.

3. RESULTS AND DISCUSSION

3.1. Characterization of the TLE/PEG/Ag/AgO NPs

By employing HRTEM, XRD, and FTIR techniques, we thoroughly examined the surface and chemical attributes of the synthesized TLE/PEG/Ag/AgO NPs. A noteworthy application aimed at advancing image analysis involves leveraging artificial intelligence (AI) for surface analysis. Within this investigation, HRTEM imaging of the fabricated NPs was conducted using a dual 8-bit RGB colored mode, subsequently applied to the AI-assisted TEM micrograph of the TLE/PEG/Ag/AgO NPs. In Figure 1, the TEM micrograph and the AI-assisted TEM micrograph of TLE/PEG/Ag/AgO NPs were presented.

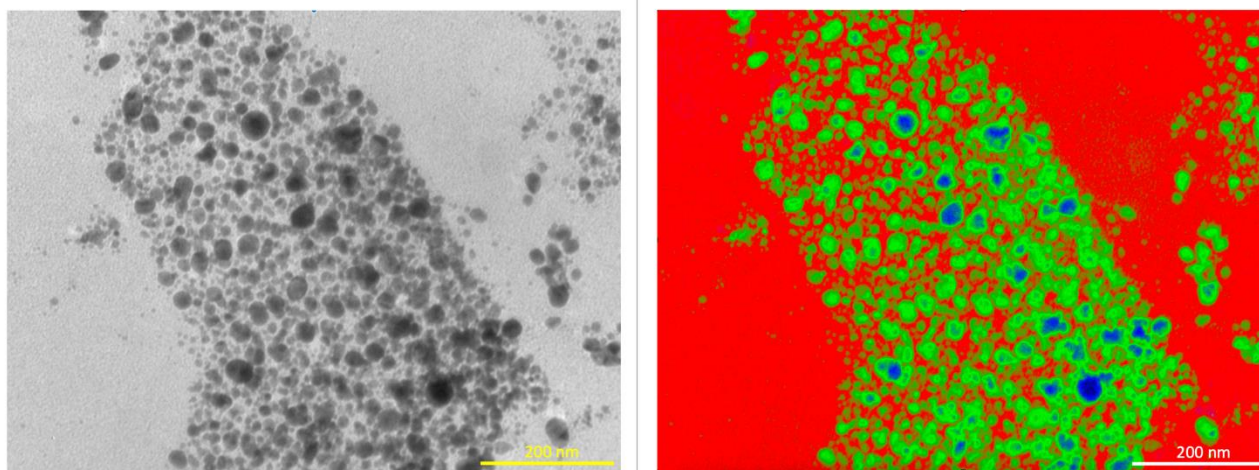


Figure 1: (a) TEM micrograph and (b) AI-assisted TEM micrograph of TLE/PEG/Ag/AgO NPs.

The homogeneous dispersion of Ag/AgO NPs within the TLE/PEG matrix is confirmed by TEM analysis, as shown in Fig. 1(a), demonstrating a homogenous particle distribution. According to TEM results, we observed that the NPs have a spherical geometry, and their diameters vary between 10-20 nm. However, considering that NPs below 10 nm are difficult to image, a digital image processing

approach was applied by applying ImageJ software to TEM images to overcome this difficulty (Fig. 1(b)). With this method, the morphology and diameters of the green/blue colored NPs could be determined more easily and effectively. The advantages provided by the ImageJ digital image processing approach helped us achieve more sensitive and precise results, especially in the detection of Ag/AgO NPs with a

diameter of sub-10 nm. In our analysis of the red, green, and blue channels within the AI-assisted TEM digital image using RGB evaluation, we observed that agglomerated Ag/AgO NPs were identified in the blue channel. Concurrently, the green-colored channel highlighted the presence of more uniformly distributed Ag/AgO NPs. The decreasing intensity of

the green color suggested that the Ag/AgO NPs may have an undetectable particle diameter. In the literature, image-processing software supported by artificial intelligence is suggested as an economical method for detecting nanostructures by evaluating microscopic results (34,35).

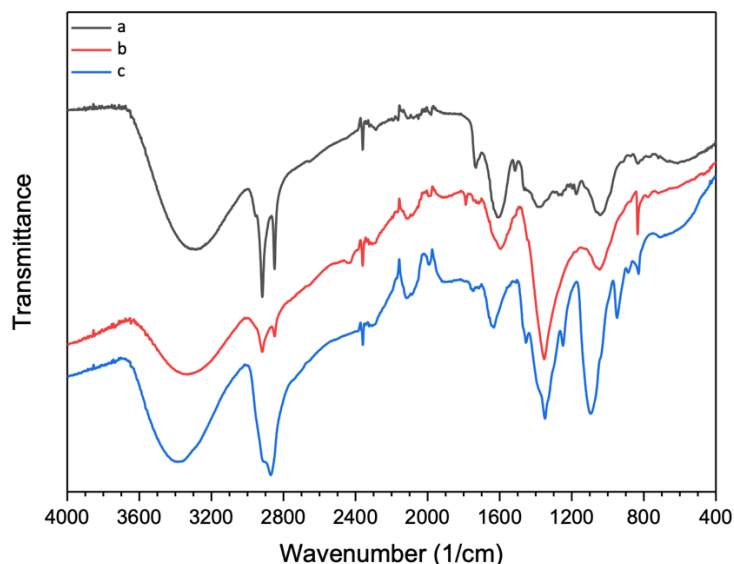


Figure 2: FTIR spectra of (a) TLE, (b) TLE/PEG, and (c) TLE/PEG/Ag/AgO NPs.

The TLE/PEG/Ag/AgO nanoparticles were found to have possessed unique functional groups according to the FTIR technique. Fig. 2 displayed the FTIR spectra of TLE, TLE/PEG, and TLE/PEG/Ag/AgO NPs. The FTIR results of TLE (Fig. 2.a) revealed distinctive peaks at specific wavenumbers: 3314 cm^{-1} (OH stretching), 2917 cm^{-1} (-CH symmetric stretching band), 2850 cm^{-1} (-CH asymmetric stretching band), 1606 cm^{-1} (C-O stretching), and 1042 cm^{-1} (C-O stretching vibrations). Additionally, a cluster of bands between 1293 to 1175 cm^{-1} corresponds to C-O-C, C-O, and O-H groups (36). In Fig. 2.b, the FTIR spectra of the TLE/PEG, it was found to have the characteristic bands at 3400 cm^{-1} (OH stretching), 2918 cm^{-1} (-CH symmetric stretching band), 2849 cm^{-1} (-CH asymmetric stretching band), 1595 cm^{-1} (C-O stretching), and 1045 cm^{-1} (C-O stretching vibrations). In this study, we attributed the low-intensity peak around 2917 cm^{-1} -2850 cm^{-1} and the highly intense peak at 1045 cm^{-1} to the formation of the prepared TLE/PEG polymeric blend (37). In Fig. 2.c, depicting the FTIR spectra of the TLE/PEG/Ag/AgO NPs, characteristic bands were identified at 3400 cm^{-1} (OH stretching), 2902 cm^{-1} (-CH symmetric stretching band), 2871 cm^{-1} (-CH asymmetric stretching band), 1663 cm^{-1} (C-O stretching), 1095 cm^{-1} (C-O stretching vibrations), 830 cm^{-1} (Ag-O), 713 cm^{-1} (Ag-O), and 535 cm^{-1} (Ag-O) (38). Compared with the FTIR spectrum of TLE/PEG, the spectrum of TLE/PEG/Ag/AgO NPs

shows observable shifts in the C-O stretching peak (from 1595 to 1663 cm^{-1}) and peaks (from 1045 to 1095 cm^{-1}). Additionally, the FTIR spectrum of TLE/PEG/Ag/AgO NPs exhibits a more intense hydroxyl peak of around 3400 cm^{-1} . The weak broadband at 2120 cm^{-1} in the FTIR spectrum of TLE/PEG/Ag/AgO NPs may be attributed to -CO-Ag (39).

These changes suggest that the NPs are synthesized and stabilized by carboxyl groups. In summary, the FTIR results of TLE, TLE/PEG, and TLE/PEG/Ag/AgO NPs show small differences; all exhibit the characteristic FT-IR spectrum of TLE/PEG. This indicates that the TLE/PEG encapsulates the NPs, effectively covering the TLE/PEG. These findings are consistent with the XRD results.

X-ray diffraction pattern analysis was used to confirm the crystallinity and phase purity of the synthesized TLE/PEG/Ag/AgO NPs, as shown in Fig. 3. The XRD data showed the effective production of TLE/PEG/Ag/AgO NPs. The cubic crystal structure of Ag NPs was identified as the source of the diffraction peaks at 2θ values of 38.24° (1 1 1), 44.50° (2 0 0), 64.76° (2 2 0), and 77.65° (3 1 1) (ICDD Card No. 01-087-0718) (40). AgO NPs' tetragonal crystal structure was also identified by peaks at 2θ values of 32.45° (2 0 2), 55.02° (2 2 4), and 67.50° (2 0 6) (ICDD Card No. 01-076-1489) (41).

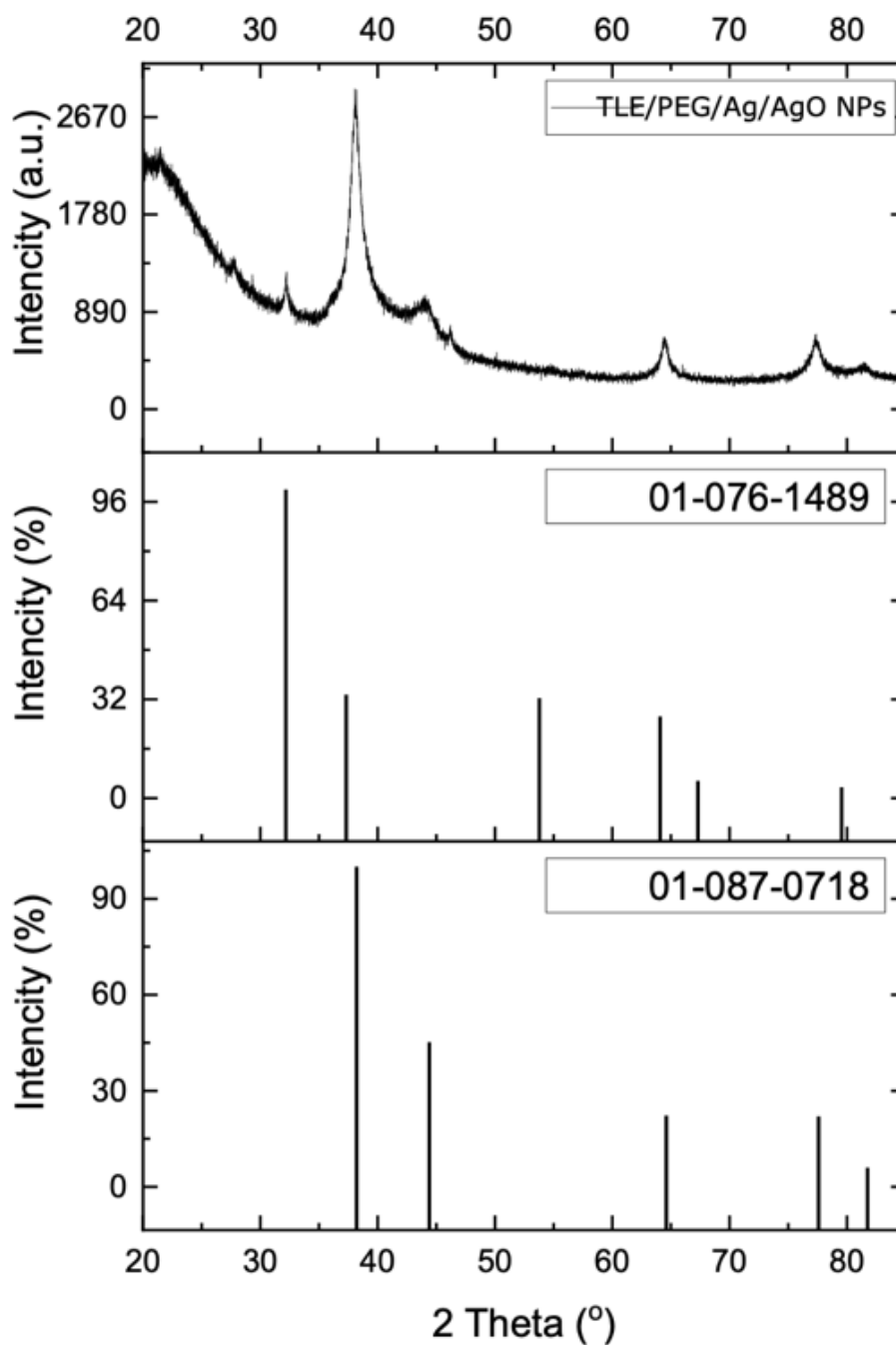


Figure 3: XRD graph of TLE/PEG/Ag/AgO NPs.

3.2. Green TLE/PEG/Ag/AgO NPs-based digital image colorimetric sensor for the detection of H₂O₂

This study employed an innovative digital image colorimetric sensor based on TLE/PEG/Ag/AgO NPs

for the detection of H₂O₂. The digital colorimetric outcomes were analyzed through cumulative RGB histograms, and subsequently, each sample image (H₂O₂, acetone, hexane, toluene, glucose, and IPA) was quantified using Pantone color values.

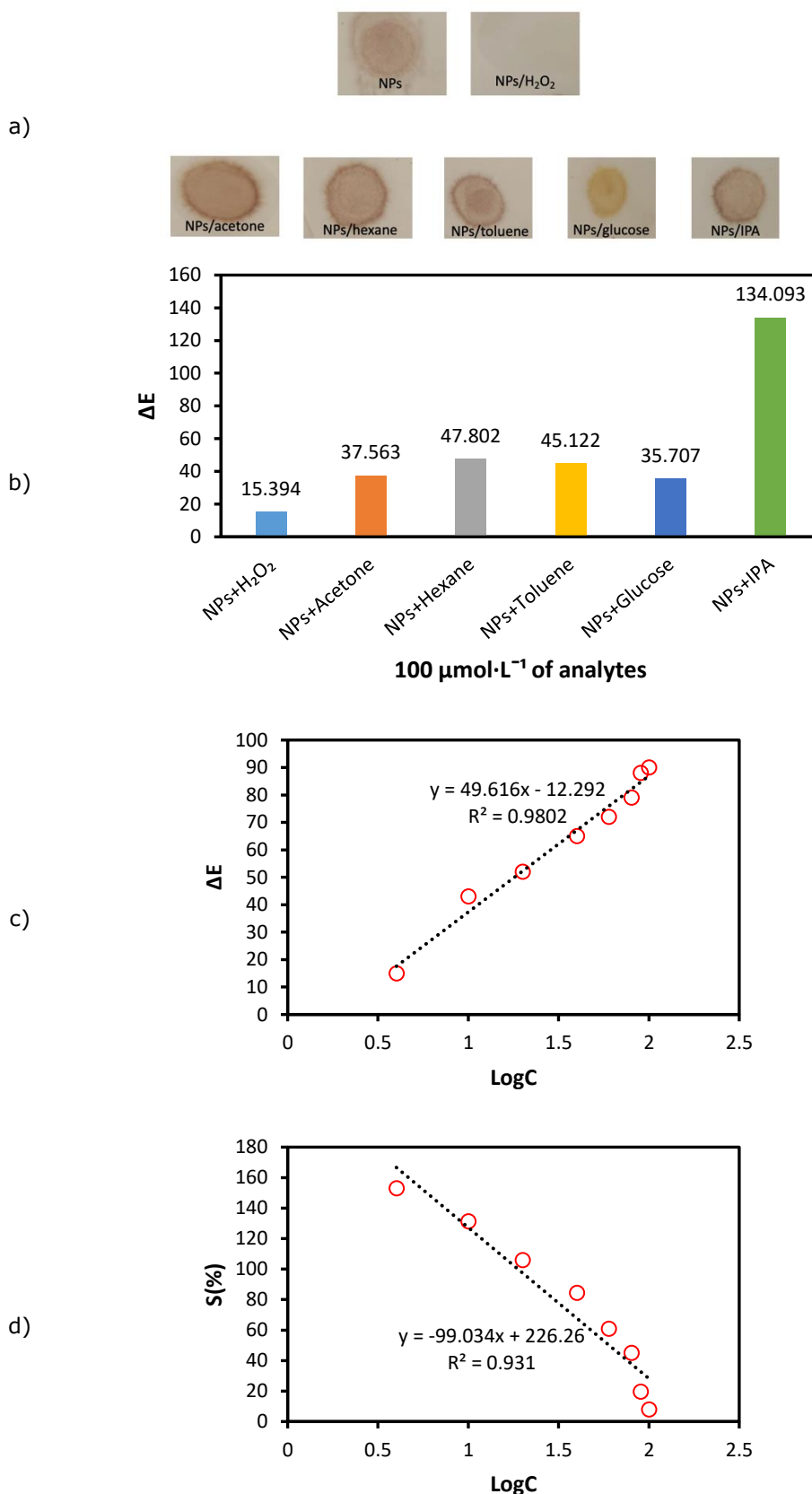


Figure 4: a) and b) Selectivity of the TLE/PEG/Ag/AgO NPs-based sensor in 100.0 μmol/L of different analytes such as H₂O₂, acetone, hexane, toluene, glucose, and IPA, the graphs of c) Log C–ΔE and (d) Log C–S (%) in a concentration range of 2.0 to 100.0 μmol/L of H₂O₂.

Figure 4 displayed various studies that demonstrated the selectivity of the TLE/PEG/Ag/AgO NPs-based sensor. The sensor's behavior towards several analytes, such as H₂O₂, acetone, hexane, glucose, and IPA, each at a concentration of 100.0

μmol/L, was depicted in Figure 4.a. The TLE/PEG/Ag/AgO NPs-based sensor's overall selectivity was summarized in Figure 4.b, highlighting its capacity for discrimination over a range of analytes and concentrations. Additional

evidence of the selectivity was provided by the graphical displays in Figures 4.c and 4.d, which showed the relationship between Log C- ΔE and Log C-S (%), respectively.

In this study, also, the color change of the analyte and the response of the colorimetric sensor were also characterized by the rate of change of the blue color (ΔB) in the RGB color channels. In control experiments, since there was no change in the blue color channel between TLE/PEG (B channel value: 155) and TLE/PEG + H₂O₂ (B channel value: 155), this was determined as the control group. Additionally, the blue color change it caused on other analytes is presented in Table 2. As can be seen, the extract containing NPs provided a higher change rate in the blue color value when applied to H₂O₂. This comparison also showed that the NPs-free extract is ineffective in detecting H₂O₂.

Table 2: Changes in blue color intensity across studied analytes.

Sample + Analyte	ΔB values
TLE + H ₂ O ₂	0
TLE/PEG + H ₂ O ₂	0
TLE/PEG/Ag/AgO NPs + H ₂ O ₂	38
TLE/PEG/Ag/AgO NPs + Acetone	20
TLE/PEG/Ag/AgO NPs + Hexane	11
TLE/PEG/Ag/AgO NPs + Toluene	7
TLE/PEG/Ag/AgO NPs + Glucose	28
TLE/PEG/Ag/AgO NPs + IPA	17

In this study, it was focused on investigating the detection of additional compounds such as IPA, H₂O₂, acetone, hexane, toluene, and glucose. The TLE/PEG/Ag/AgO NPs-based sensor, known for its sensitivity and selectivity, was utilized with the user-friendly ImageJ software. In the presence of H₂O₂, the sensitive detection exhibited a noticeable color shift, while other analytes (acetone, hexane, toluene,

glucose, and IPA) displayed a substantial color change (Fig. 4.a). The digital colorimetric TLE/PEG/Ag/AgO NPs-based sensor employed the RGB method for the detection of H₂O₂.

According to Fig.4a-d, the sample color changed from green to yellow after one minute and within the range of 2.0 to 100.0 $\mu\text{mol/L}$ of H₂O₂ concentration. The TLE/PEG/Ag/AgO NPs-based sensor's ΔE values for H₂O₂, acetone, hexane, toluene, glucose, and IPA were determined to be 15, 37, 47, 45, 35, and 134, respectively, based on the RGB data. Additionally, throughout a broad concentration range of 2.0 to 100.0 $\mu\text{mol/L}$, the ΔE values of the TLE/PEG/Ag/AgO NPs-based sensor showed a colorimetric change, ranging from 15 to 90. The TLE/PEG/Ag/AgO NPs-based sensor's colorimetric data demonstrated its extremely selective performance, with an LOD of 0.27 $\mu\text{mol/L}$ within the concentration range of 2.0 to 100.0 $\mu\text{mol/L}$. Table 3 presented various performance parameters of the Ag-contributing nanostructures designed for H₂O₂ sensing.

The experimental results reported in this work demonstrated the great potential of the TLE/PEG/Ag/AgO NPs-based sensor for H₂O₂ detection. With its large dynamic range of 2.0 to 100.0 $\mu\text{mol/L}$, sensitivity, and selectivity, it emerged as a promising option for various real-world applications. The sensor's high sensitivity was crucial for accurate detection even at low concentrations, as evidenced by its low LOD of 0.27 $\mu\text{mol/L}$. The digital colorimetric data further emphasized the sensor's rapid response, qualifying it for real-time applications. In particular, the noticeable color shift within a minute was remarkable. The colorimetric variations over a wide concentration range and the reported ΔE values for several analytes demonstrate the versatility and potential for selective detection of the sensor.

Table 3: Various performance parameters of the Ag-contributing nanostructures designed for H₂O₂ sensing.

Electrode	Potential (V)	Measurement Range (mmol/L)	LOD ($\mu\text{mol/L}$)	Sensitivity ($\mu\text{A/mM/cm}^2$)	Reference
AgNPs/3DG	-0.65	0.03-16.21	14.9	1.094	(41)
AgNPs-rGO-PANI/GCE	-0.4	0.01-1	0.05	14.7	(42)
AgNPs/CS/GE	-0.3	-	6.6	115.2	(43)
AgNPs/N-G/GCE	-0.3	0.1-126	1.2	4.46	(44)
AgNPs-rGO/ITO	-0.3	0.1-100	1.6	-	(45)
Ag/PSi/CPE	-0.45	0.0016-0.5	0.45	-	(46)
Nafion/Gr-CCS-AgNPs/GCE	-0.2	0.02-5.02	2.49	-	(47)
MWCNT/Ag nanohybrids/Gold electrode	-0.2	0.05-17	0.5	1.42	(48)
GC/rGO-Nf@Ag	-0.65	1-30	0.535	0.4508	(49)
AgNPs-MWCNT-rGO/GCE	-0.35	0.1-100	0.9	-	(50)
AgNPs/Cu-TCPP/CCE	-0.25	0.0037-5.8	1.2	21.6	(51)
AgNPs/NDs/GCE	-0.2	0.0001-0.0034	0.01	0.00159	(52)
MnO ₂ -Ag nanowire/GCE	-0.5	0.1-4	0.24	-	(53)
(PDA/AgNPs)/GCE	-0.6	0.05-1.75	6.5	-	(54)
TiO ₂ NTs/rGO/AgNPs/GCE	-0.6	0.05-15.5	2.2	1151.98	(55)
SPE/rGO@CeO ₂ -AgNPs	-0.3	0.0005-12	0.21	-	(56)
Ag-TiN/SMS	-0.3	0.00005-2.1	0.0077	33.25	(57)
Ag-HNTs-MnO ₂	-0.3	0.002-4.71	0.7	11.9	(58)

4. CONCLUSION

In conclusion, the TLE/PEG/Ag/AgO NPs-based sensor has demonstrated significant promise for H₂O₂ detection, as indicated by the study's findings. Its noteworthy features, encompassing a broad dynamic range from 2.0 to 100.0 µmol/L, excellent sensitivity, and remarkable selectivity, are underscored by the published experimental results. With a low LOD at 0.27 µmol/L, the sensor emerges as a valuable choice for numerous practical applications, showcasing its capacity for precise detection even at minute concentrations. The colorimetric data's swift response, including a discernible color shift within a minute, further accentuates its potential for real-time applications. The observed ΔE values for various analytes and the demonstrated adaptability in colorimetric fluctuations over a wide concentration range highlight the sensor's effectiveness and promise for selective detection. Overall, these results affirm that the TLE/PEG/Ag/AgO NPs-based sensor is a viable and versatile tool for accurate cancer biomarker (H₂O₂) detection, with implications for a variety of real-world applications.

5. CONFLICT OF INTEREST

There is no conflict of interest.

6. REFERENCES

- Xu J, Ma J, Peng Y, Cao S, Zhang S, Pang H. Applications of metal nanoparticles/metal-organic frameworks composites in sensing field. *Chinese Chem Lett* [Internet]. 2023 Apr;34(4):107527. Available from: [<URL>](#).
- Qanash H, Bazaid AS, Alharazi T, Barnawi H, Alotaibi K, Shater ARM, et al. Bioenvironmental applications of myco-created bioactive zinc oxide nanoparticle-doped selenium oxide nanoparticles. *Biomass Convers Biorefinery* [Internet]. 2024 Aug 1;14(15):17341–52. Available from: [<URL>](#).
- Lu N, Shao C, Li X, Miao F, Wang K, Liu Y. CuO nanoparticles/nitrogen-doped carbon nanofibers modified glassy carbon electrodes for non-enzymatic glucose sensors with improved sensitivity. *Ceram Int* [Internet]. 2016 Jul;42(9):11285–93. Available from: [<URL>](#).
- Zhang W, Hong C, Pan C. Polymerization-Induced Self-Assembly of Functionalized Block Copolymer Nanoparticles and Their Application in Drug Delivery. *Macromol Rapid Commun* [Internet]. 2019 Jan 2;40(2):1800279. Available from: [<URL>](#).
- Hulsey S, Absar S, Choi H. Investigation of simultaneous ultrasonic processing of polymer-nanoparticle solutions for electrospinning of nanocomposite nanofibers. *J Manuf Process* [Internet]. 2018 Aug;34:776–84. Available from: [<URL>](#).
- Afzali M, Mostafavi A, Shamspur T. Developing a novel sensor based on ionic liquid molecularly imprinted polymer/gold nanoparticles/graphene oxide for the selective determination of an anti-cancer drug imiquimod. *Biosens Bioelectron*

[Internet]. 2019 Oct;143:111620. Available from: [<URL>](#).

- Alavi M, Varma RS. Phytosynthesis and modification of metal and metal oxide nanoparticles/nanocomposites for antibacterial and anticancer activities: Recent advances. *Sustain Chem Pharm* [Internet]. 2021 Jun;21:100412. Available from: [<URL>](#).
- Shashiraj KN, Hugar A, Kumar RS, Rudrappa M, Bhat MP, Almansour AI, et al. Exploring the Antimicrobial, Anticancer, and Apoptosis Inducing Ability of Biofabricated Silver Nanoparticles Using *Lagerstroemia speciosa* Flower Buds against the Human Osteosarcoma (MG-63) Cell Line via Flow Cytometry. *Bioengineering* [Internet]. 2023 Jul 10;10(7):821. Available from: [<URL>](#).
- Dissanayake NM, Arachchilage JS, Samuels TA, Obare SO. Highly sensitive plasmonic metal nanoparticle-based sensors for the detection of organophosphorus pesticides. *Talanta* [Internet]. 2019 Aug;200:218–27. Available from: [<URL>](#).
- Zhai D, Liu B, Shi Y, Pan L, Wang Y, Li W, et al. Highly Sensitive Glucose Sensor Based on Pt Nanoparticle/Polyaniline Hydrogel Heterostructures. *ACS Nano* [Internet]. 2013 Apr 23;7(4):3540–6. Available from: [<URL>](#).
- Ghosh G. Early detection of cancer: Focus on antibody coated metal and magnetic nanoparticle-based biosensors. *Sensors Int* [Internet]. 2020;1:100050. Available from: [<URL>](#).
- Gholami M, Koivisto B. A flexible and highly selective non-enzymatic H₂O₂ sensor based on silver nanoparticles embedded into Nafion. *Appl Surf Sci* [Internet]. 2019 Feb;467–468:112–8. Available from: [<URL>](#).
- Teodoro KBR, Migliorini FL, Christinelli WA, Correa DS. Detection of hydrogen peroxide (H₂O₂) using a colorimetric sensor based on cellulose nanowhiskers and silver nanoparticles. *Carbohydr Polym* [Internet]. 2019 May;212:235–41. Available from: [<URL>](#).
- Ismail M, Khan MI, Akhtar K, Khan MA, Asiri AM, Khan SB. Biosynthesis of silver nanoparticles: A colorimetric optical sensor for detection of hexavalent chromium and ammonia in aqueous solution. *Phys E Low-dimensional Syst Nanostructures* [Internet]. 2018 Sep;103:367–76. Available from: [<URL>](#).
- Mohammed GM, Hawar SN. Green Biosynthesis of Silver Nanoparticles from *Moringa oleifera* Leaves and Its Antimicrobial and Cytotoxicity Activities. Ali S, editor. *Int J Biomater* [Internet]. 2022 Sep 19;2022:4136641. Available from: [<URL>](#).
- Judith Vijaya J, Jayaprakash N, Kombaiyah K, Kaviyarasu K, John Kennedy L, Jothi Ramalingam R, et al. Bioreduction potentials of dried root of Zingiber officinale for a simple green synthesis of silver nanoparticles: Antibacterial studies. *J Photochem Photobiol B Biol* [Internet]. 2017 Dec;177:62–8. Available from: [<URL>](#).
- Aldosary SK, El-Rahman SNA, Al-Jameel SS, Alromihi NM. Antioxidant and antimicrobial activities

- of *Thymus vulgaris* essential oil contained and synthesis thymus (*Vulgaris*) silver nanoparticles. *Brazilian J Biol* [Internet]. 2023;83:e244675. Available from: [<URL>](#).
18. Hambardzumyan S, Sahakyan N, Petrosyan M, Nasim MJ, Jacob C, Trchounian A. *Origanum vulgare* L. extract-mediated synthesis of silver nanoparticles, their characterization and antibacterial activities. *AMB Express* [Internet]. 2020 Dec 5;10(1):162. Available from: [<URL>](#).
19. Mirzajani F, Askari H, Hamzelou S, Schober Y, Römpf A, Ghassempour A, et al. Proteomics study of silver nanoparticles toxicity on *Oryza sativa* L. *Ecotoxicol Environ Saf* [Internet]. 2014 Oct;108:335–9. Available from: [<URL>](#).
20. Singh A, Jain D, Upadhyay MK, Khandelwal N, Verma HN. Green synthesis of silver nanoparticles using *Argemone Mexicana* leaf extract and evaluation of their antimicrobial activities. *Dig J Nanomater Biostructures* [Internet]. 2010;5(2):483–9. Available from: [<URL>](#).
21. He Y, Wei F, Ma Z, Zhang H, Yang Q, Yao B, et al. Green synthesis of silver nanoparticles using seed extract of *Alpinia katsumadai*, and their antioxidant, cytotoxicity, and antibacterial activities. *RSC Adv* [Internet]. 2017;7(63):39842–51. Available from: [<URL>](#).
22. Malabadi RB, Mulgund GS, Meti NT, Nataraja K, Vijaya Kumar S. Antibacterial activity of silver nanoparticles synthesized by using whole plant extracts of *Clitoria ternatea*. *Res Pharm* [Internet]. 2012;2(4):10–21. Available from: [<URL>](#).
23. Anushaa A, Pushpa A, Vijaya KG, Thippareddy K. Green synthesis of non-cytotoxic silver nanoparticles using *Solanum nigrum* leaves extract with antibacterial properties. *GSC Biol Pharm Sci* [Internet]. 2021 Jun 30;15(3):262–71. Available from: [<URL>](#).
24. Lu L, Zhuang Z, Fan M, Liu B, Yang Y, Huang J, et al. Green formulation of Ag nanoparticles by *Hibiscus rosa-sinensis*: Introducing a navel chemotherapeutic drug for the treatment of liver cancer. *Arab J Chem* [Internet]. 2022 Feb;15(2):103602. Available from: [<URL>](#).
25. Zayed MF, Mahfoze RA, El-kousy SM, Al-Ashkar EA. In-vitro antioxidant and antimicrobial activities of metal nanoparticles biosynthesized using optimized *Pimpinella anisum* extract. *Colloids Surfaces A Physicochem Eng Asp* [Internet]. 2020 Jan;585:124167. Available from: [<URL>](#).
26. Yasmin H. M, Veerendra C. Y. Synthesis of *Coccinia grandis* (L.) Voigt extract's silver nanoparticles and its in vitro antidiabetic activity. *J Appl Pharm Sci* [Internet]. 2021 Aug 5;11(8):108–15. Available from: [<URL>](#).
27. Renuka R, Devi KR, Sivakami M, Thilagavathi T, Uthrakumar R, Kaviyarasu K. Biosynthesis of silver nanoparticles using *phyllanthus emblica* fruit extract for antimicrobial application. *Biocatal Agric Biotechnol* [Internet]. 2020 Mar;24:101567. Available from: [<URL>](#).
28. Niluxsshun MCD, Masilamani K, Mathiventhan U. Green Synthesis of Silver Nanoparticles from the Extracts of Fruit Peel of *Citrus tangerina*, *Citrus sinensis*, and *Citrus limon* for Antibacterial Activities. *Ciccarella G*, editor. *Bioinorg Chem Appl* [Internet]. 2021 Feb 2;2021:695734. Available from: [<URL>](#).
29. Hussain M, Raja NI, Mashwani Z, Naz F, Iqbal M, Aslam S. Green synthesis and characterisation of silver nanoparticles and their effects on antimicrobial efficacy and biochemical profiling in *Citrus reticulata*. *IET Nanobiotechnology* [Internet]. 2018 Jun 21;12(4):514–9. Available from: [<URL>](#).
30. Mogole L, Omwoyo W, Viljoen E, Moloto M. Green synthesis of silver nanoparticles using aqueous extract of *Citrus sinensis* peels and evaluation of their antibacterial efficacy. *Green Process Synth* [Internet]. 2021 Dec 7;10(1):851–9. Available from: [<URL>](#).
31. Basavegowda N, Rok Lee Y. Synthesis of silver nanoparticles using Satsuma mandarin (*Citrus unshiu*) peel extract: A novel approach towards waste utilization. *Mater Lett* [Internet]. 2013 Oct;109:31–3. Available from: [<URL>](#).
32. Sekkat A, Liedke MO, Nguyen VH, Butterling M, Baiutti F, Sirvent Veru J de D, et al. Chemical deposition of Cu₂O films with ultra-low resistivity: correlation with the defect landscape. *Nat Commun* [Internet]. 2022 Sep 9;13(1):5322. Available from: [<URL>](#).
33. Engel L, Benito-Altamirano I, Tarantik KR, Pannek C, Dold M, Prades JD, et al. Printed sensor labels for colorimetric detection of ammonia, formaldehyde and hydrogen sulfide from the ambient air. *Sensors Actuators B Chem* [Internet]. 2021 Mar;330:129281. Available from: [<URL>](#).
34. Thompson NBA, O'Sullivan SE, Howell RJ, Bailey DJ, Gilbert MR, Hyatt NC. Objective colour analysis from digital images as a nuclear forensic tool. *Forensic Sci Int* [Internet]. 2021 Feb;319:110678. Available from: [<URL>](#).
35. Karakuş S, Özbaş F, Baytemir G, Taşaltın N. Cubic-shaped *corylus colurna* extract coated Cu₂O nanoparticles-based smartphone biosensor for the detection of ascorbic acid in real food samples. *Food Chem* [Internet]. 2023 Aug;417:135918. Available from: [<URL>](#).
36. Boughendjioua H, Mezedjeri NEH, Idjouadiene I. Chemical constituents of Algerian mandarin (*Citrus reticulata*) essential oil by GC-MS and FT-IR analysis. *Curr Issues Pharm Med Sci* [Internet]. 2020 Dec 1;33(4):197–201. Available from: [<URL>](#).
37. Georgieva M, Gospodinova Z, Keremidarska-Markova M, Kamenska T, Gencheva G, Krasteva N. PEGylated Nanographene Oxide in Combination with Near-Infrared Laser Irradiation as a Smart Nanocarrier in Colon Cancer Targeted Therapy. *Pharmaceutics* [Internet]. 2021 Mar 22;13(3):424. Available from: [<URL>](#).
38. Rita A, Sivakumar A, Dhas SSJ, Dhas SAMB. Structural, optical and magnetic properties of silver oxide (AgO) nanoparticles at shocked conditions. *J*

- Nanostructure Chem [Internet]. 2020 Dec 24;10(4):309–16. Available from: [<URL>](#).
39. Bhagyaraj S, Krupa I. Alginate-Mediated Synthesis of Hetero-Shaped Silver Nanoparticles and Their Hydrogen Peroxide Sensing Ability. *Molecules* [Internet]. 2020 Jan 21;25(3):435. Available from: [<URL>](#).
40. Jaiswal KK, Banerjee I, Dutta S, Verma R, Gunti L, Awasthi S, et al. Microwave-assisted polycrystalline Ag/AgO/AgCl nanocomposites synthesis using banana corm (rhizome of *Musa sp.*) extract: Characterization and antimicrobial studies. *J Ind Eng Chem* [Internet]. 2022 Mar;107:145–54. Available from: [<URL>](#).
41. Zhan B, Liu C, Shi H, Li C, Wang L, Huang W, et al. A hydrogen peroxide electrochemical sensor based on silver nanoparticles decorated three-dimensional graphene. *Appl Phys Lett* [Internet]. 2014 Jun 16;104(24):243704. Available from: [<URL>](#).
42. Kumar V, Gupta RK, Gundampati RK, Singh DK, Mohan S, Hasan SH, et al. Enhanced electron transfer mediated detection of hydrogen peroxide using a silver nanoparticle-reduced graphene oxide-polyaniline fabricated electrochemical sensor. *RSC Adv* [Internet]. 2018;8(2):619–31. Available from: [<URL>](#).
43. Dodevska T, Vasileva I, Denev P, Karashanova D, Georgieva B, Kovacheva D, et al. Rosa damascena waste mediated synthesis of silver nanoparticles: Characteristics and application for an electrochemical sensing of hydrogen peroxide and vanillin. *Mater Chem Phys* [Internet]. 2019 Jun;231:335–43. Available from: [<URL>](#).
44. Tian Y, Wang F, Liu Y, Pang F, Zhang X. Green synthesis of silver nanoparticles on nitrogen-doped graphene for hydrogen peroxide detection. *Electrochim Acta* [Internet]. 2014 Nov;146:646–53. Available from: [<URL>](#).
45. Moradi Golsheikh A, Huang NM, Lim HN, Zakaria R, Yin CY. One-step electrodeposition synthesis of silver-nanoparticle-decorated graphene on indium-tin-oxide for enzymeless hydrogen peroxide detection. *Carbon N Y* [Internet]. 2013 Oct;62:405–12. Available from: [<URL>](#).
46. Ensafi AA, Rezaloo F, Rezaei B. Electrochemical sensor based on porous silicon/silver nanocomposite for the determination of hydrogen peroxide. *Sensors Actuators B Chem* [Internet]. 2016 Aug;231:239–44. Available from: [<URL>](#).
47. Wang H, Wang H, Li T, Ma J, Li K, Zuo X. Silver nanoparticles selectively deposited on graphene-colloidal carbon sphere composites and their application for hydrogen peroxide sensing. *Sensors Actuators B Chem* [Internet]. 2017 Feb;239:1205–12. Available from: [<URL>](#).
48. Zhao W, Wang H, Qin X, Wang X, Zhao Z, Miao Z, et al. A novel nonenzymatic hydrogen peroxide sensor based on multi-wall carbon nanotube/silver nanoparticle nanohybrids modified gold electrode. *Talanta* [Internet]. 2009 Dec 15;80(2):1029–33. Available from: [<URL>](#).
49. Yusoff N, Rameshkumar P, Mehmood MS, Pandikumar A, Lee HW, Huang NM. Ternary nanohybrid of reduced graphene oxide-nafion/silver nanoparticles for boosting the sensor performance in non-enzymatic amperometric detection of hydrogen peroxide. *Biosens Bioelectron* [Internet]. 2017 Jan;87:1020–8. Available from: [<URL>](#).
50. Lorestani F, Shahnava Z, Mn P, Alias Y, Manan NSA. One-step hydrothermal green synthesis of silver nanoparticle-carbon nanotube reduced-graphene oxide composite and its application as hydrogen peroxide sensor. *Sensors Actuators B Chem* [Internet]. 2015 Mar;208:389–98. Available from: [<URL>](#).
51. Ma J, Bai W, Zheng J. Non-enzymatic electrochemical hydrogen peroxide sensing using a nanocomposite prepared from silver nanoparticles and copper (II)-porphyrin derived metal-organic framework nanosheets. *Microchim Acta* [Internet]. 2019 Jul 27;186(7):482. Available from: [<URL>](#).
52. Habibi B, Jahanbakhshi M. Sensitive determination of hydrogen peroxide based on a novel nonenzymatic electrochemical sensor: silver nanoparticles decorated on nanodiamonds. *J Iran Chem Soc* [Internet]. 2015 Aug 4;12(8):1431–8. Available from: [<URL>](#).
53. Han Q, Ni P, Liu Z, Dong X, Wang Y, Li Z, et al. Enhanced hydrogen peroxide sensing by incorporating manganese dioxide nanowire with silver nanoparticles. *Electrochem Commun* [Internet]. 2014 Jan;38:110–3. Available from: [<URL>](#).
54. Wang F, Han R, Liu G, Chen H, Ren T, Yang H, et al. Construction of polydopamine/silver nanoparticles multilayer film for hydrogen peroxide detection. *J Electroanal Chem* [Internet]. 2013 Oct;706:102–7. Available from: [<URL>](#).
55. Wang W, Xie Y, Xia C, Du H, Tian F. Titanium dioxide nanotube arrays modified with a nanocomposite of silver nanoparticles and reduced graphene oxide for electrochemical sensing. *Microchim Acta* [Internet]. 2014 Aug 27;181(11–12):1325–31. Available from: [<URL>](#).
56. Yao S, Xu J, Wang Y, Chen X, Xu Y, Hu S. A highly sensitive hydrogen peroxide amperometric sensor based on MnO₂ nanoparticles and dihexadecyl hydrogen phosphate composite film. *Anal Chim Acta* [Internet]. 2006 Jan;557(1–2):78–84. Available from: [<URL>](#).
57. Chu Y, Huang Z, Wang X, Zhou M, Zhao F. Highly dispersed silver imbedded into TiN microspheres for electrochemical detecting of hydrogen peroxide. *Sci Rep* [Internet]. 2020 Dec 17;10(1):22126. Available from: [<URL>](#).
58. Zhang S, Sheng Q, Zheng J. Synthesis of Ag-HNTs-MnO₂ nanocomposites and their application for nonenzymatic hydrogen peroxide electrochemical sensing. *RSC Adv* [Internet]. 2015;5(34):26878–85. Available from: [<URL>](#).